Vienna Congress on Recent Advances in
Earthquake Engineering and Structural Dynamics 2013 (VEESD 2013)
C. Adam, R. Heuer, W. Lenhardt & C. Schranz (eds)
28-30 August 2013, Vienna, Austria
Paper No. 294

Theoretical and experimental research on liquefaction susceptibility of sand

S. A. Savidis[1,2], D. Aubram[1], C. Carow[1], R. Glasenapp[1], W. Schepers[2]

[1] Chair of Soil Mechanics and Foundation Engineering, Technische Universität Berlin, Germany
[2] GuD CONSULT GmbH, Berlin, Germany

Abstract. Laboratory test devices are presented capable of simulating appropriately the response of water saturated sand to transient loads. In particular, liquefaction phenomena are well reproduced. For the execution of numerical analyses a powerful constitutive model for water saturated sand and a two-phase finite element are presented. The capabilities of the constitutive model are verified by simulation of cyclic laboratory tests. Two boundary value problems are solved with the presented simulation tools. The results prove that the complex behaviour of the soil skeleton, its interaction with the pore water and certain liquefaction phenomena due to cyclic loading can be simulated well.

Keywords: Liquefaction; Coupled fluid-solid FEM; Bounding Surface Plasticity, Simple shear and triaxial tests

1 INTRODUCTION

In 373 B.C. the Greek city of Helike submerged into the Mediterranean Sea during a strong earthquake. Geoarcheological investigations (Ferentinos and Papatheodorou 2005) revealed a large scale landslide triggered by liquefaction to be the cause of the submerging. Though humans have been threatened by the catastrophic consequences of liquefaction for millennia, scientific research of the subject started only after two devastating earthquakes in 1964 in Japan and Alaska which caused large damage due to liquefaction.

In recent times research on liquefaction triggering events was extended to cyclic loads, e. g. at offshore structures, as well as the rising of ground water levels during the renaturation of opencast pits.

This paper presents the current experimental and numerical research on the mechanical behaviour of water-saturated sand subject to cyclic loads. It will be shown that the results can be applied to improve the prediction of large deformations during pore water accumulation. The first part focuses on the experimental investigations. In the second part the methods and procedures that are necessary for numerical simulations of liquefaction are presented. This is followed by a presentation of two boundary value problems to show the potential as well as the restrictions of the presented methods.

2 EXPERIMENTAL RESEARCH

2.1 Test equipment

For studying liquefaction of sand undrained element tests as well as test with constant specimen volume can be used. Cyclic triaxial tests as well as simple shear tests are suitable test types.

During cyclic triaxial tests cyclic loads can be applied to cylindrical specimens subjected to an arbitrary axisymmetric stress and to arbitrary drainage conditions. The cyclic change of loads is accomplished by either changing the cell pressure and the excess pore pressure, or by changing the piston force. That is, the cyclic loading is applied by changing the principal stress. For liquefaction analyses of sand it must be ensured that the soil specimen is 100 % saturated such that during cyclic loading and closed drainage no change of volume does occur. The pore water pressure then depends only on density, initial stress state, ratio of cyclic stress amplitude to mean effective stress, and grain size distribution.

In a simple shear apparatus, instead of performing truly undrained tests with fully saturated specimens, constant volume tests using dry specimens are performed as an equivalent substitute in order to circumvent water sealing problems which the simple shear apparatus is prone to. In a constant volume test the lateral displacement of the specimen is restrained. Hence, the volume of the specimen can be kept constant by controlling the vertical stress applied by the piston. During shearing in a simple shear apparatus the principal axes rotate, which is observed at many practical geotechnical applications. The non-uniform stress distribution due to the shear stress-free lateral confinement of the specimen, however, is a disadvantage of the simple shear apparatus if compared to the cyclic triaxial apparatus, because neither the orientation of the principal axes nor the amplitude of the principal stress can well be established.

At TU Berlin two cyclic triaxial apparatuses and two cyclic simple shear apparatuses are available for research on liquefaction phenomena. Furthermore, a resonant column/torsional shear apparatus is available for the determination of dynamic soil properties.

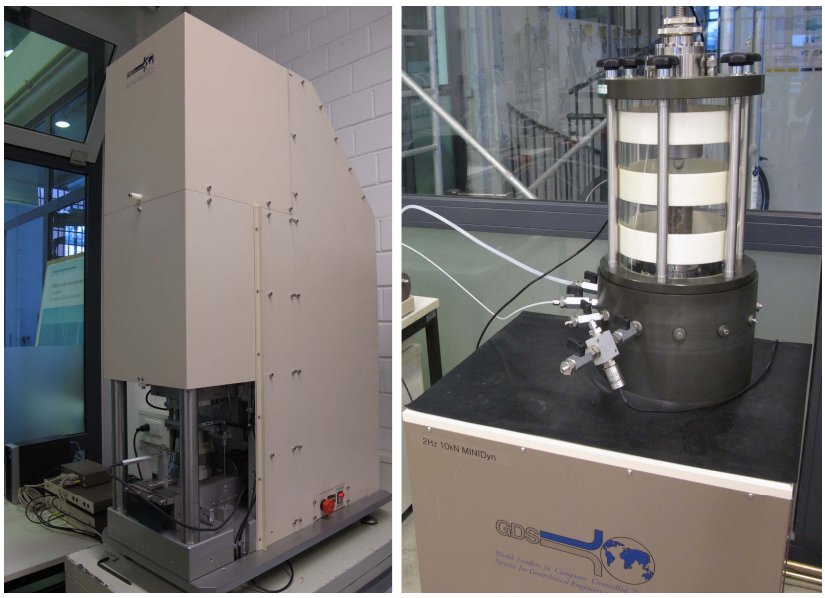

Figure 1: Test equipment for element tests at the soil mechanics laboratory of TU Berlin. Left: simple shear apparatus. Right: cyclic triaxial apparatus

2.2 Liquefaction phenomena in laboratory tests

A large number of constant volume simple shear tests of sand have been performed in the past within various research activities. In figure 2 the result of such a test on medium dense Berlin Sand is shown. During cyclic shear the specimen tends to respond contractive, but due to the enforced constant volume the effective stress is reduced and so is the shear strength. Effective stress drops to a minimum within a few cycles, and continued cyclic loading leads to alternating dilatant and contractive re-

sponse. Deformations grow with each cycle but remain finite. This phenomenon is known as "cyclic mobility".

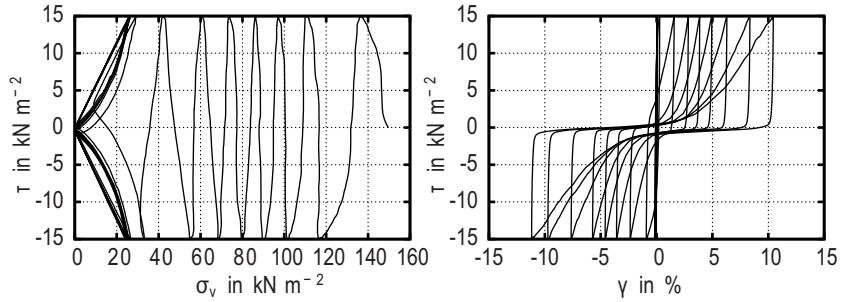

Figure 2: constant volume cyclic simple shear test on Berlin Sand ($\sigma_{v,0}$ = 150 kN/m², $I_{D,0}$ = 33 %)

For a loosely deposited sand, however, the failure of the specimen occurs much more sudden as can be seen from figure 3 where the result of a constant volume simple shear test with loose sand is shown. The sudden failure is a characteristic property of liquefaction.

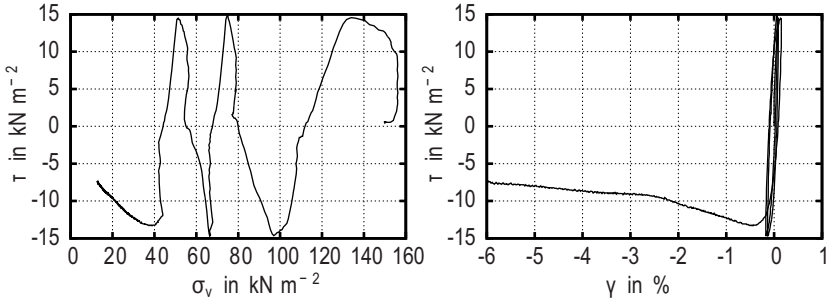

Figure 3: constant volume cyclic simple shear test on North Sea Sand ($\sigma_{v,0}$ = 150 kN/m², $I_{D,0}$ = 66 %)

In order to assess the liquefaction potential of non-cohesive soils liquefaction curves are a useful tool. To obtain a liquefaction curve several cyclic tests with different cyclic stress ratios have to be performed. The cyclic stress ratio is then plotted over the number of cycles N_{Liq} at which the effective stress drops to zero (figure 4). Such a curve is called liquefaction curve regardless of true liquefaction or cyclic mobility is observed during the tests.

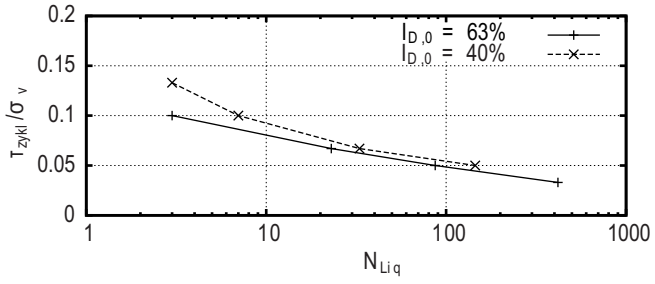

Figure 4: Liquefaction curves for Berlin Sand after simple shear tests at $\sigma_{v,0}$ = 150 kN/m² with $I_{D,0}$ = 40 % and $I_{D,0}$ = 63 %

3 NUMERICAL SIMULATION

For the numerical simulation of liquefaction phenomena by means of finite element computations the mechanical properties of the soil skeleton as well as the interaction with the pore water must be properly modelled. That requires a constitutive model for the soil skeleton on the one hand, and a coupled fluid-solid finite element for saturated soil on the other hand.

3.1 Constitutive model for the soil skeleton

For the realistic simulation of the mechanical properties of the soil skeleton the powerful CSSA model (Critical State SAnd model) after (Li 2002) was selected here. It evolved from the bounding-surface plasticity scheme after (Dafalias 1986), which was extended by the Generalized Plasticity concept after (Pastor et al. 1990).

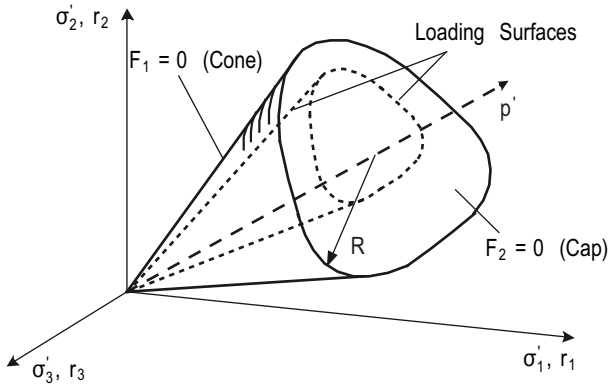

Figure 5: Bounding surface and loading surface of the CSSA constitutive model

The CSSA model defines two bounding surfaces, F_1, and F_2. They are shown in figure 5 in the effective stress space. Bounding surface F_1 is an irregular cone enclosing the hydrostatic stress axis ($\sigma_1 = \sigma_2 = \sigma_3$). It is bounded by a cap, which is the second bounding surface F_2. The actual stress state is always located on the intersection of the two loading surfaces inside the bounding surfaces, and is mapped onto the bounding surfaces. During monotonic loading the loading surfaces coincide with the bounding surfaces.

Another important feature of the CSSA model is the dependency of the dilatancy on the loading history, as well as on the actual stress state and density. Dilatancy is used here as a kinematic variable and is defined as the ratio of volumetric strain to deviatoric strain. The change of dilatancy during continued shearing can be characterized by comparing the actual stress and density state with the critical state. The critical state is defined as the state at which relative density and stress do not change during continued shearing.

In (Li 1998) it was shown that all critical states of a particular sand are located on a straight line if plotted as in figure 6. This line is called "Critical State Line" (CSL). The plot represents the so called compression space, with the void ratio e on the vertical axis and the stress ratio $(p'/p_a)^{\xi}$ on the horizontal axis, with p' the mean effective stress, p_a the atmospheric pressure at sea level, and ξ a constitutive parameter. In figure 6 the CSL of a particular sand is given by the constitutive parameters e_Γ and λ_c,with e_c the void ratio at critical state. The CSSA model simulates the dilatancy of sand based on the distance ψ from the CSL in compression space.

$$\psi = e - e_c = e - \left[e_\Gamma - \lambda_c (p'/p_a)^{\xi}\right] \tag{1}$$

The dilatancy function D_1 for the bounding surface F_1 is then defined as

$$D_1 = \frac{d_1}{M_c\ g(\theta)} \left(M_c\ g(\theta) \exp(m\,\psi) \sqrt{\frac{\bar{\rho}_1}{\rho_1}} - R \right) \tag{2}$$

with d_1, M_c, and m constitutive parameters, and $\bar{\rho}_1$ and ρ_1 distance measures of the mapping. The functions $g(\theta)$, with θ the Lode angle, determines the shape of the bounding surface, and R is an invariant of the stress ratio tensor $r_{ij} = s_{ij}/p'$ with s_{ij} the deviator of the stress tensor.

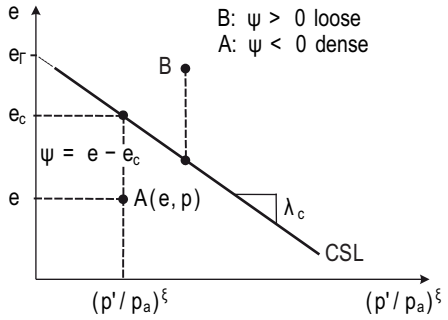

Figure 6: Critical state line and state parameter ψ

The CSSA model was implemented as a user defined material in ANSYS (Rackwitz 2003). It is called during execution of the global Newton-Raphson algorithm. To verify the implementation and to demonstrate the capabilities of the CSSA model, laboratory tests with Berlin Sand have been simulated. Figure 7 shows, as an example, the simulation of a simple shear test. The simulation results match the laboratory tests in stress space quite well.

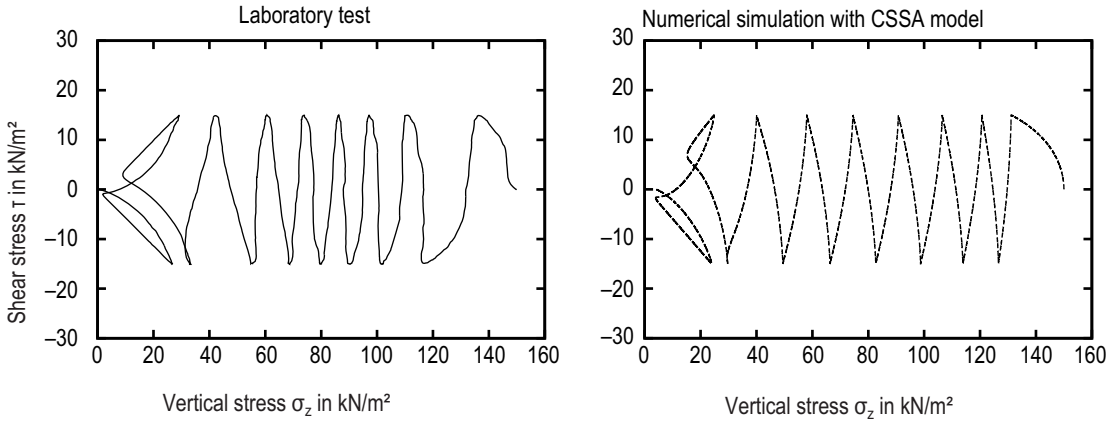

Figure 7: Undrained cyclic simple shear test with Berlin sand. Left: laboratory test. Right: Numerical simulation with the CSSA model (I_D = 66 %, σ_{z0} = 150 kN/m², τ_{max} = 15 kN/m²)

3.2 Two-phase finite element

For the coupled FE analysis of grain skeleton and pore fluid the two-phase model after Zienkievicz and Shiomi 1984 is applied. The porous medium is considered as a fully saturated continuum. Water and grain skeleton are homogeneously mixed, that is, they cannot be discerned separately. Physical variables at a certain point in space are mean values of the surrounding volume. Single grains as well as the pore water are assumed to be incompressible. Primary variables are the displacements of the

grain skeleton **u** and the pore water pressure p_w. Considering the principle of effective stress after Terzaghi the momentum balance of the mixture can be written as

$$\mathbf{L}^T\left(\boldsymbol{\sigma} - \mathbf{m}\, p_w\right) + \rho\,\mathbf{b} = \rho\,\ddot{\mathbf{u}} \tag{3}$$

with $\boldsymbol{\sigma}$ the effective stress vector, ρ the density of water saturated soil, **b** the acceleration vector of the mixture, $\mathbf{m}^T = (1, 1, 1, 0, 0, 0)$ and **L** the divergence operator.

Applying Darcy's law the mass balance of both phases can be written as

$$\mathbf{m}\,\mathbf{L}^T\,\dot{\mathbf{u}} - \nabla^T \frac{\mathbf{K}_p}{\eta_w} \nabla p_w + \nabla^T \frac{\mathbf{K}_p}{\eta_w} \rho_w\, \mathbf{b} = 0 \tag{4}$$

with ρ_w the density of water. The permeability matrix $\mathbf{K}_p$ depends on the viscosity of water and the permeability of the grain skeleton, which is assumed to be isotropic.

The discretisation of eqs. (3) and (4) is presented in (Taşan et al. 2010). For the displacements triquadratic shape functions with 20 nodes per element have been used, while for the pore pressure trilinear shape functions with 8 nodes per elements have been used. The acronym "u20p8" is used for this element type. The increased order of the displacement's shape functions ensures the numerical stability of the element compared to an element with equal shape functions for displacements and pore pressure.

4 APPLICATIONS

Two boundary value problems, namely a soil stratum subjected to harmonic base excitation and an embankment subjected to seismic excitation, are presented to demonstrate the potential as well as the restrictions of the numerical tools with respect to liquefaction analyses. A boundary value problem similar to the former has been investigated previously using single phase elements (Savidis et al. 2005, Savidis et al. 2006)

4.1 Soil stratum subject to harmonic excitation

The soil stratum shown in figure 8 consists of 50 m loosely deposited Berlin sand over infinitely rigid and impermeable rock. The stratum has an infinite lateral expansion. It is excited at the bottom by an excitation spatially constant but harmonic in time. Material parameters for Berlin sand are taken from (Rackwitz 2003). The stratum is permeable at the top.

Due to the applied assumptions it suffices to model a single column of the soil stratum with finite elements. Horizontal as well as vertical displacements of nodes at the same elevation are restrained such that pure shear deformation is enforced.

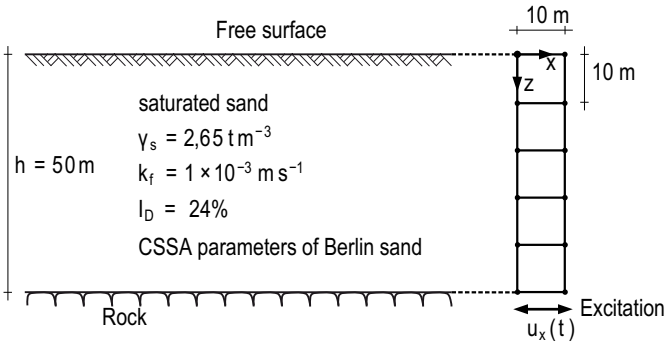

Figure 8: Properties and finite element mesh of a soil stratum

As the first step, the initial stress state for the dynamic computations is computed by subjecting the stratum to gravity. As the second step, the harmonic excitation (amplitude $\hat{u}_x = 0.1$ m, frequency f = 1 Hz, duration $t_{max} = 5$ s) is applied. After that, the soil column consolidates for 295 s. The results in terms of pore water pressure and displacements during and immediately after the excitation are shown in figure 9.

In figure 9 $p_{tot} = \frac{1}{3}(\sigma_x + \sigma_y + \sigma_z)$ denotes the mean total stress. That is, the ratio p_w/p_{tot} represents the contribution of excess pore pressure to the mean total stress. If that ratio becomes equal to one, the effective stress vanishes and liquefaction is initiated.

From figure 9a it becomes obvious that liquefaction occurs first at the bottom of the stratum. Due to the loss of shear strength the propagation of the shear wave from bottom to top is compromised. Therefore, in the upper part of the stratum the soil does not fully liquefy. At the top, however, full liquefaction occurs again, because the overburden pressure is very low. Consequently, liquefaction occurs near the top of the stratum at rather low excess pore pressure levels.

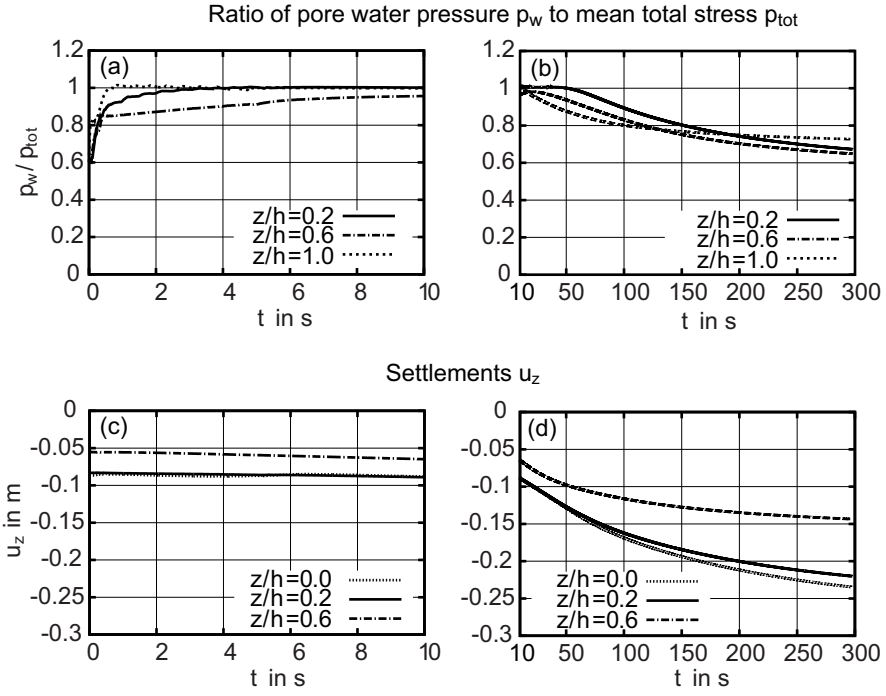

Figure 9: Soil stratum response. Left: during excitation (t < 5 s) and immediately after (5 s ≤ t ≤ 10 s). Right: during consolidation

On the right hand side of figure 9 the post-excitation response of the stratum is shown. The excess pore water pressure is dissipated due to the drainage at the free surface (figure 9b). While the settlements are negligible during the excitation because of the long drainage path (figure 9c), the effective stress in the soil skeleton significantly increases during the post-excitation period, and so do the settlements (figure 9d).

4.2 Embankment subjected to seismic excitation

The second example is an infinitely long, fully saturated embankment of loose sand subjected to an seismic excitation, as shown in figure 10. The symmetric embankment has a height of 6 m, a width of 39 m at the base and a slope angle of 20°. All surfaces are permeable, except for the base which is assumed to be impermeable. Material parameters for Berlin sand are taken from (Rackwitz 2003).

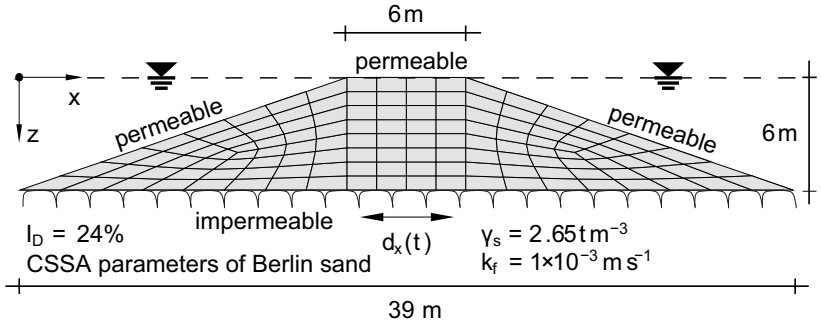

Figure 10: Embankment subjected to seismic excitation

As the first step the initial stress state was imposed by applying gravity. During the second step a displacement was applied spatially constant at the base. As the acceleration time series the leading 20 s of the San Fernando earthquake of 09. February 1971 in Los Angeles, California, was selected (Seekins et al. 1992). The displacement and acceleration time history of the excitation are shown in figure 11a and 11b, respectively.

In figure 11c the pressure ratio time history of several points on the line of symmetry of the embankment is plotted. While at the embankment base the pore water pressure changes little over time, strong oscillations occur concurrently with the largest excitation amplitudes near the crest. At z/h = 0.25 the pore water pressure ratio approaches $p_w/p_{tot} = 1$, i.e. liquefaction is almost initiated. Most probably pressure waves in the pore water are reflected at the free boundaries.

The settlements, as plotted in figure 11d, emerge immediately and increase continuously. Therefore, only small portions of the effective stress are temporarily transferred to the pore water.

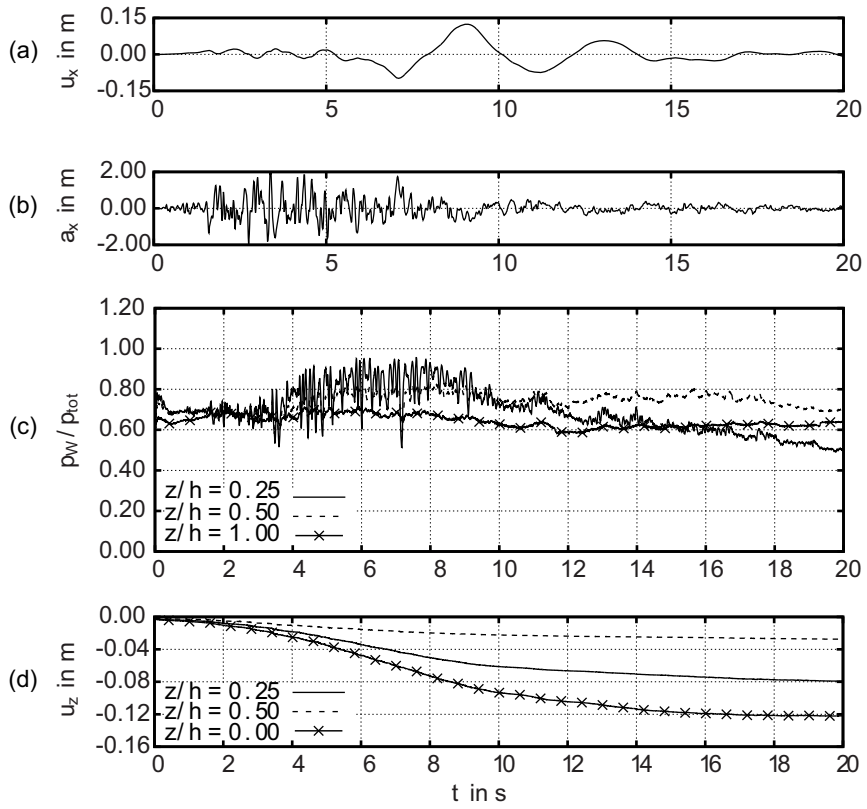

Figure 11: Embankment subjected to seismic excitation

SUMMARY AND OUTLOOK

Laboratory test devices have been presented which are capable of simulating the response of satured sands to transient loading appropriately. In particular, liquefaction phenomena are well reproduced, though not all contributing factors, like the arrangement of load cycles, have been investigated yet.

For the execution of numerical analyses a powerful constitutive model for water saturated sand (CSSA) and a two-phase finite element (u20p8) have been presented. The capabilities of the CSSA model are verified by back analysis of cyclic laboratory tests. By solving two boundary value problems it has been shown that the complex response of the soil skeleton and its interaction with the pore water can be reproduced numerically, which include the simulation of liquefaction phenomena due to cyclic and seismic loads.

Nevertheless, despite the capabilities of the presented methods for solving certain problem types, several aspects of coupled analysis of pore fluid and soil skeleton are still subject of current research activities at TU Berlin, e. g. partial saturation, large displacements, as well as the impact of certain construction methods like driving, shaking, and injecting, amongst others.

ACKNOWLEDGEMENTS

Financial support by DFG for the research presented in this paper under grant SA 310/27-1 and DFG FOR 1136 is greatly acknowledged.

REFERENCES

Ferentinos, A, and Papatheodorou G (2005). The diappearance of Helike-Classical Greece: New geological evidence. *33. International Geological Congress*, Oslo, Norway, 6–14 August 2008. English summary available at http://www.cprm.gov.br/33IGC/1352910.html.

Dafalias, Y. F. (1986). Bounding Surface Plasticity I: Mathematical Foundation and Hypoplasticity. *Journal of Engineering Materials* **112**: 996–987

Li, X. S. (1998). Linear Representation of Steady-State Line. *Journal of Geotechnical and Geoenvironmental Engineering* **124**: 1215–1217

Li, X. S. (2002). A sand model with state-dependent dilatancy. *Géotechnique* **52**: 173–186

Pastor, M., Zienkiewicz, O. C., and Chan, A. H. C. (1990). Generalized Plasticity and dthe Modeling of Soil Behaviour. *International Journal for Numerical and Analytical Methods in Geomechanics* **14**: 151–190

Rackwitz, F. (2003). Numerische Untersuchungen zum Tragverhalten von Zugpfählen und Zugpfahlversuchen in Sand auf der Grundlage von Probebelastungen. *Dissertation, Technische Universität Berlin* (in German)

Savidis, S. A., Aubram, D., Rackwitz, F. and Schepers, W. (2005) Non-Linear Constitutive Equations for Sand under Cyclic Loading and Application to Geotechnical Earthquake Engineering. In: Gazetas, G. (Ed.): *Proceedings 1st Greek-Japan Workshop: Seismic Design, Observation and Retrofit of Foundations*. Athens, Greece, 11-12 October 2005

Savidis, S. A., Aubram, D., Rackwitz, F. and Schepers, W. (2006) Numerische Modellierung des mechanischen Verhaltens von Sand unter zyklischer Belastung und ihre Anwendung im Erdbebeningenieurwesen. In: Ruge, P. and Graf, W. (Eds.): *Tagungsband 10. Dresdner Baustatik-Seminar: Neue Bauweisen - Trends in Statik und Dynamik*, pp. 489–502. Dresden, Germany, 29 September 2006 (in German)

Seekins, L. C., Brady, G. A., Carpenter, C. and Brown, N. (1992). Digitized Strong-Motion Accelerograms of North and Central American Earthquakes 1933–1986. USGS Digital Data Series DDS-7. http://nsmp.wr.usgs.gov/data_sets/ncae.html

Taşan, H. E., Rackwitz, F., and Savidis, S.A. (2010). Porenwasserdruckakkumulation bei zyklisch horizontal belasteten Monopiles mit großen Durchmessern. *Bautechnik* **87**: 449–461 (in German)

Zienkiewicz, O. C. and Shiomi, T. (1984). Dynamic behavior of saturated porous media; the generalized Biot formulation and its numerical solution. *International Journal for Numerical and Analytical Methods in Geomechanics* **8**: 71–96